CrOx-mediated Performance Enhancement of Ni/NiO-Mg:SrTiO3 in Photocatalytic Water Splitting

Kai Han
University of Twente
Diana Haiber
Arizona State University
Julius Knöppel
FZ Julich
Caroline Lievens
University of Twente
Serhiy Cherevko
Forschungszentrum Jülich https://orcid.org/0000-0002-7188-4857
Peter A. Crozier
Arizona State University
Guido Mul (G.mul@utwente.nl)
University of Twente
Bastian Mei
University of Twente https://orcid.org/0000-0002-3973-9254

Article

Keywords: Photocatalytic water splitting, co-catalyst, stability, in situ ICP-MS, SrTiO3

Posted Date: February 15th, 2021

DOI: https://doi.org/10.21203/rs.3.rs-142709/v1

Abstract

By photodeposition of small quantities of CrOx on SrTiO3-based semiconductors, doped with aliovalent Mg(II) and functionalized with Ni/NiO catalytic nanoparticles (economically significantly more viable than commonly used Rh catalysts), an increase in Apparent Quantum Efficiency (AQEs) from ~10% to 26% in overall water splitting was obtained. Deposition of CrOx also significantly enhances the stability of Ni/NiO nanoparticles in production of hydrogen, allowing sustained operation, even in intermittent cycles of illumination. In situ elemental analysis of the water constituents during, or after photocatalysis, shows that after CrOx deposition, dissolution of Ni-ions from Ni/NiO-Mg:SrTiO3 is significantly suppressed, explaining the stabilizing effect of CrOx on water splitting performance. State-of-the-art electron microscopy and EDX and EELS analyses demonstrate that upon preparation, CrOx is photodeposited in the vicinity of several, but not all, Ni/NiO particles. This implies the formation of a Ni-Cr mixed metal oxide, which is highly effective in water reduction. Inhomogeneities in the interfacial contact, evident from differences in contact angles between Ni/NiO particles and the Mg:SrTiO3 semiconductor, likely affect the probability of reduction of Cr(VI)-species during synthesis by photodeposition, explaining the observed inhomogeneity in the spatial CrOx distribution. Furthermore, by comparison with undoped SrTiO3, Mg-doping appears essential in providing such favorable interfacial contact and to establish the beneficial effect of CrOx. This study suggests that the performance of semiconductors can be significantly improved if inhomogeneities in interfacial contact between semiconductors and highly effective catalytic nanoparticles can be resolved by (surface) doping and improved synthesis protocols.

Introduction

The performance of $SrTiO_3$ (STO) based photocatalysts in the light-driven overall splitting of water to H_2 and O_2 has recently been significantly improved by aliovalent doping of the perovskite material by Al or Mg, and surface-modification by deposition of appropriate co-catalysts such as Rh/CrO_x.[1–7] In fact for Rh/CrO_x-modified Al:STO an apparent quantum efficiency (AQY) of up to 96% (UV-LED illumination) and solar to hydrogen efficiency (STH) of 0.65% have been reported.[6] Triggered by this successful development, the first large scale flat-plate reactors are evaluated in long-term stability measurements under realistic conditions.[7] The outstanding properties of aliovalently doped Al:STO have been assigned to removal (lower density) of Ti^{3+} mid-gap states (favorable recombination sites), which was recently confirmed by a combined experimental and theoretical investigation.[4] Similarly, for Mg:STO composites (AQY of 10% promoted with Ni/NiO), some of us proposed that Mg reduces the density of free-charge carriers leading to a favorable surface-space-charge layer, promoting the oxygen evolution reaction.[3] Still co-catalyst modification is mandatory to facilitate water reduction at the surface of these aliovalently doped $SrTiO_3$-based composites. Particularly, co-catalysts consisting of chromium-oxide and typically Rh[8–10] have been widely utilized to induce photocatalytic activity of $SrTiO_3$ or Al:$SrTiO_3$ photocatalysts. In this context CrO_x is generally proposed to form thin film coatings on active hydrogen evolution catalysts, preventing the parasitic oxygen reduction reaction.[6,8,11–13] Despite the frequently employed

picture of a core-shell structure, recent studies demonstrate that formation of mixed metal oxides containing CrO_x and e.g. Rh, is also likely.[1,14,15]

Ni/NiO co-catalysts are another type of often employed co-catalysts enabling photocatalytic overall water splitting. Similarly to CrO_x in Rh/CrO_x, a NiO-shell is believed to prevent oxygen reduction to occur on the metallic Ni core.[16] Additionally, it has been reported that spatially separated particles of Ni and NiO_x promote the formation of hydrogen and oxygen, respectively.[17,18] Recently, we revealed significant and unfavorable transients in the hydrogen production rate using Ni/NiO-modified $SrTiO_3$.[18] Dynamics in composition and structure of the Ni/NiO core–shell particles correlate well with the observed transients in gas evolution.[19] Certainly, stabilization of the active phase(s) of the Ni/NiO co-catalyst system is required to fully exploit the potential of the system, which is potentially more economically viable than Rh-based formulae.[19,20]

Here, we report novel insight in the extent and origin of the effect of CrO_x prepared by reductive photodeposition on unprecedented enhancement of the photocatalytic activity and stability of Ni/NiO_x-Mg:$SrTiO_x$ composite photocatalysts. High-resolution transmission electron microscopy with energy dispersive X-ray or electron energy loss spectroscopy (HR-TEM-EDX/EELS) reveals a spatial CrO_x distribution primarily in the vicinity of the Ni/NiO_x particles. The EDX and EELS data are explained by the formation of mixed CrO_x/NiO_x phases. Moreover, (in-situ) Inductively coupled plasma mass spectrometry/optical emission spectrometry (ICP-MS/OES) illustrates a significant reduction in leaching/dissolution of Ni-ions from CrO_x/NiO_x phases as compared to Ni/NiO_x during cyclic operation. It will be discussed that Mg synergistically promotes the activity of the composite photocatalyst, likely by providing a favorable interfacial contact between the semiconductor (Mg:$SrTiO_3$) and the Ni/NiO_x particles. The insights provided will guide research devoted to increasing performance, including stability, of photocatalysts.

Experimental Methods

Materials

$SrTiO_3$ was prepared by mixing and grinding of stoichiometric amounts of $SrCO_3$ (99.995 % Sigma-Aldrich) and Rutile TiO_2 (99.995% Sigma-Aldrich) and subsequent calcination at 1100 °C for 10 h. Mg:$SrTiO_3$ was prepared following a two-step procedure. A detailed description is provided elsewhere.[3] Briefly, $MgSO_4$ was mixed with Rutile (TiO_2) and treated at 800 ^oC in air. Obtained powders were converted to Mg:$SrTiO_3$ by mixing and grinding with $SrCO_3$ and calcination at 1100 ^oC for 10 h. The ratio of materials was adjusted to enable synthesis of $Sr_{1.25}Mg_{0.3}TiO_x$, hereafter identified by Mg:$SrTiO_3$. Detailed characterization (see also results section on HR-TEM/EDX and ICP analysis) shows that the

actual Mg content is lower in the active Mg:$SrTiO_3$ composite. This is caused by significant dissolution of Mg upon suspension in water, needed for washing, Ni impregnation, and photodeposition of CrO_x.

To deposit core/shell-type Ni/NiO co-catalysts,[19] 0.2 g Mg:$SrTiO_3$ or $SrTiO_3$ was dispersed in 20 mL of an aqueous solution of $Ni(NO_3)_2$. The obtained mixture was stirred for 2 h and afterwards the solution was evaporated till dryness (80 °C, overnight). The Ni-precursor was converted to NiO at 400 °C (10 K min^{-1} ramp rate) in synthetic air (30 mL min^{-1}), followed by treatment in 5% H_2/N_2 (80 ml min^{-1}) at 500 °C (at 10 K min^{-1}) for 10 h. Core/shell Ni/NiO structures were obtained by cooling the tube furnace to 130 °C in 5% H_2/N_2 (80 ml min^{-1}), before introducing N_2 and subsequently air (30 ml min^{-1}) for 1 h. The Ni loading was verified to be 1 wt% by XRF analysis.

Modification with chromium oxide was achieved by photodeposition. Briefly, 0.1 g of Ni/NiO-Mg:$SrTiO_3$ was dispersed in 10 mL of a 10 mM $K_2Cr_2O_4$ solution (pH ~5). The resulting slurry was illuminated for 3 hours using a UV LED light source (365 nm, 3.2 mW cm^{-2}). Afterwards the obtained powder was separated from solution by filtration and dried at 80 °C for 12 h. The amount of CrO_x was verified to be 0.2 wt% in all cases by X-ray fluorescence (XRF) analysis.

Photocatalytic activity experiments

The photocatalytic activity of the synthesized photocatalysts (25 mg catalyst in 25 mL DI water) was measured using a continuously stirred tank reactor (30 mL cuvette, 402.013-OG obtained from Hellma), equipped with a gas-tight lid.[21] Products were stripped from the reactor with a continuous He flow of 10 mL min^{-1}, unless otherwise specified, and analyzed using a gas chromatograph equipped with a highly sensitive Pulsed Discharge Detector (Interscience). Apparent quantum efficiencies were determined using 365 nm LED illumination (Roithner LaserTechnik), with a measured intensity of 1.9 mW cm^{-2}. The area of illumination was 2.25 cm^2 for all experiments and oxygen was removed from the solution prior to illumination by He purge overnight.

Characterization

XRD measurements were performed with a Bruker D2 (Cu K_α source) Diffractometer. Raman spectroscopy was performed at room temperature using an Avantes AvaRaman spectrometer, equipped with a 785 nm laser. A Philips PW 1480 analyzer was used for XRF analysis. XPS was measured using a Quantera SXM from Physical Electronics using monochromatic Al Kα radiation (1486.6 eV). All spectra were calibrated to the carbon C1s peak at 284.8 eV. Detailed TEM analysis was performed at different magnifications. Survey imaging of the fresh Ni/NiO-Mg:$SrTiO_3$ and CrO_x-modified Ni/NiO-Mg:$SrTiO_3$ was performed using a JEOL 2010F microscope, operating at 200-kV. Local elemental analysis was obtained from a probe-corrected JEOL ARM200F scanning TEM (STEM), operating at 200 kV, equipped with a

windowless EDAX X-ray detector and a Gatan Enfinium EELS spectrometer. High resolution TEM (HRTEM) imaging at 300kV was performed with an aberration-corrected FEI Titan instrument.

In situ ICP-MS measurements were performed in a photoelectrochemical scanning flow cell (SFC) connected to an inductively coupled plasma mass spectrometer (ICP-MS) (NexION 300X, Perkin Elmer).[22] Daily calibration was performed with a four-point calibration at concentrations of (0; 0.5; 1; 5) µg l^{-1} for Mg, Ti, Ni, Cr and Sr with standard solutions (Merck Certipur) mixed in DI water (Merck Milipore). Sc(Mg, Ti), Co(Ni) and Y(Cr, Sr) solutions at 10 µg l^{-1} in 1% HNO_3 were used as internal standards. Several photocatalysts (Ni/NiO_x-$SrTiO_3$, Ni/NiO_x-Mg:$SrTiO_3$ and CrO_x-modified Ni/NiO_x-Mg:$SrTiO_3$) were immobilized by drop casting from aqueous suspension on glassy carbon substrates. The loading of every individual measurement spot was ~15 µg and a spot size of around 1.2 mm was used (Figure 1).[22–24] A flow of liquid DI water of 186 µL min^{-1} was introduced, and the water composition was analyzed after contact with the sample. The flow was maintained for 10 minutes in darkness, after which the photocatalyst was exposed to light (385 nm, 60 mW cm^{-2}, Thorlabs M385F1) for 5 minutes. Finally, the water flow was maintained for an additional 15 minutes in the dark. The Sr, Ti, Mg, and Ni-contents in the effluent were analyzed by integration over the various treatment periods (light on/off). Additionally, ICP-OES analysis (*ex situ*) of liquid aliquots taken during activity measurements were performed using a Perkin Elmer 8300dv to determine concentrations of dissolved Cr, Mg, and Ni at different stages of the reaction. Prior to the ICP-OES analysis the photocatalyst was isolated from the slurry solution by filtration, and only isolated clear solutions were used for analysis.

Results And Discussion

Performance evaluation: Overall water splitting and backreaction

The photocatalytic water splitting activities induced by UV light illumination (365 nm LED light source) of Mg:$SrTiO_3$ with either Ni/NiO_x or CrO_x-modified Ni/NiO_x co-catalysts are compared in Figure 2a.

The initially rapid increase in apparent gas production for both catalysts is due to the characteristic residence time of product gas in the reactor and feed-lines to the GC, and the time needed to reach steady state CSTR behavior. A decrease in gas production is observed for Ni/NiO_x-Mg:$SrTiO_3$ under continuous operation,[3,19] which we previously assigned to changes in oxidation state and morphology of the core/shell Ni/NiO particles in Ni/NiO_x-$SrTiO_3$. Remarkably, after CrO_x-modification the stability of the photocatalyst is significantly improved, retaining at least 90% of the steady state photocatalytic activity after 70 hours of day/night cyclic operation (5.6 µmol g^{-1} min^{-1} of H_2 is produced, see Figure **S1)**. Considering the measured photon flux of the 365 nm LED light, the apparent quantum yield (AQY) is calculated to be 26±2% for CrO_x-modified Ni/NiO-Mg:$SrTiO_3$ (for data on simulated solar illumination, see Figure **S2**).

Figure **2b** shows the effect of the presence of Mg-doping on the beneficial effect of photodeposition of CrO_x. Interestingly, CrO_x modification of Ni/NiO_x-$SrTiO_3$ hardly leads to improvement (the H_2 production yield obtained after 8 h only increases from 510 μmol•g^{-1} to 550 μmol g^{-1}), while the steady state performance of Ni/NiO_x-Mg:$SrTiO_3$ was improved by a factor of ~2 by photodeposition of CrO_x. In the absence of Mg, CrO_x furthermore has a significantly smaller positive effect on the stability (Figure S3). These observations suggest that Mg is essential to achieve the positive effect of CrO_x on the performance of Ni/NiO_x core/shell particles.[1,10]

In studies on photocatalytic water splitting, significant improvements in activity and selectivity due to CrO_x-modification are generally assigned to suppression of the unfavorable oxygen reduction reaction (ORR) by forming a protective shell around particularly Rh nanoparticles.[25] Therefore we determined the photocatalytic performance of the Mg-doped composites in the presence of exogenous oxygen (and hydrogen). In the absence of light, neither Ni/NiO_x-Mg:$SrTiO_3$ nor the CrO_x-modified Ni/NiO_x-Mg:$SrTiO_3$ photocatalyst induces (chemical) conversion of O_2. Figure **3** compares the characteristic photocatalytic performance (rate is displayed on the left y-axis and the AQY on the right y-axis) of (CrO_x-modified) Ni/NiO_x-Mg:$SrTiO_3$ when purging 80 ppm of H2 and 80 ppm of O_2. Once initiating illumination, H_2 and O_2 are produced resembling the trends observed in pure He purge (compare Figure 2). Terminating illumination results in a fast transient in gas production, and concentrations quickly stabilize to the background levels. Re-initiating illumination recovers gas production, with Ni/NiO_x-Mg:$SrTiO_3$ continuing deactivation. Since the partial pressure of oxygen in continuous flow reactors is typically low in comparison to batch-type systems,[26–28] the absence of the oxygen reduction reaction (at 80 ppm) was to be expected.[10,29]

This is further confirmed by a transient in feed gas from He to the gas containing 80 ppm of H_2, O_2 and N_2 during photocatalytic experiment (Figure **S4),** hardly showing any effect of this gas compositional change on performance. Finally, production rates of H_2 and O_2 are independent of the purge-gas flow rate (Figure **S5**),[26,28] which should not be the case if reduction of oxygen occurs.[28,30,31] Summarizing, these results show that Ni/NiO core-shell structures appear to be poor catalysts for the ORR at the concentrations relevant for the present study, and it is thus unlikely that suppression of unwanted side reactions by CrO_x deposition explains the enhanced performance of CrO_x promoted NiO_x-Mg:$SrTiO_3$.[10] Alternatively, we propose that a mixed oxide formulation of CrO_x and Ni/NiO_x (and Mg) is formed, which is highly effective in the water reduction reaction, and enhances the stability against dissolution of NiOx phases. First we will provide evidence for the formation of mixed Cr and Ni oxide phases, and will discuss the spatial distribution of CrO_x in the composite, followed by a detailed study of dissolution of NiO_x in the investigated catalytic formulations.

Materials Characterization: Localizing photodeposited CrO_x

In an attempt to localize CrO_x on the surface of the prepared photocatalysts, XRD (Figure **S6**), Raman (Figure **S7**), XPS and (HR/S)TEM were used. XRD, Raman and XPS were not able to provide any evidence of the oxidation state, nor crystal structure of CrO_x and as such CrO_x appears to be present in low quantities on the surface.

The oxidation states of the Ni/NiO_x co-catalyst on the surface of Ni/NiO_x-$Mg:SrTiO_3$ and CrO_x-modified Ni/NiO_x-$Mg:SrTiO_3$ were determined by XPS for both, as-prepared, and measured samples. In as-prepared Ni/NiO_x-$Mg:SrTiO_3$ (Figure **S8a**) the Ni $2p_{3/2}$ signal mainly consists of contributions from Ni^{2+} (NiO at 853.5 eV). A minor contribution of metallic Ni^0 (851.9 eV) is also revealed. After illumination, the width and symmetry of the Ni signal changed, which suggests that the relative contribution of Ni^{2+} (as in $Ni(OH)_2$ at 855.6 eV) is significantly enhanced as compared to Ni^0. Formation of NiOOH might also contribute to the overall peak shape. This assignment is also in agreement with the changes in the O1s signal induced by illumination (Figure **S9**).[19] In contrast, Ni and O signals of the CrO_x-modified Ni/NiO_x-$Mg:SrTiO_3$ composite show little difference, before and after illumination (Figure **S8b**), suggesting that NiO_x preserves the oxidation state (Ni^{2+} (as in $Ni(OH)_2$ at 855.6 eV) and presumably some NiOOH). In fact the dominant presence of oxidized Ni-species in the as-prepared CrO_x-modified Ni/NiO_x-$Mg:SrTiO_3$ is likely due to the applied photodepostion procedure, in which the most stable Ni oxidation state was formed.

TEM images showing the morphology of the as-prepared photocatalysts are compared in Figure **4a-d.** All materials exhibit large $Mg:SrTiO_3$ particles in the order of 100s of nanometers. Ni/NiO_x core shell particles decorate the surface throughout and are roughly 5-30 nm in size with a shell thickness of approximately 2 nm (for HRTEM images of Ni/NiO_x particles the reader is referred to Figures **S10-14**). The morphology of the supported Ni/NiO_x core-shell particles is rather heterogenous throughout each sample. Specifically, for some core-shell particles low contact angles (indicating good bonding to the support) are revealed, whereas weak interfaces with larger contact angles are observed for others.

To investigate differences in the structure of the Ni/NiO_x particles on each photocatalyst composite in more detail, both before and after undergoing photocatalytic measurements, HRTEM imaging was performed. Figure **5a** shows a typical core-shell particle as observed for CrO_x-modified Ni/NiO_x-$Mg:SrTiO_3$, being almost indistinguishable from particles analyzed in (Cr-free) Ni/NiO_x-$Mg:SrTiO_3$ (see for comparison Figures S12 and S14). In Figure **5b**, the corresponding FFT is displayed showing the presence of Ni, NiO, and $Ni(OH)_2$, in agreement with XPS analysis and previous observations reported for

Ni/NiO_x-$SrTiO_3$ composites after illumination.[19] Thus, we suggest $Ni(OH)_2$ most likely forms as a result of illumination during photodeposition of CrO_x. Using inverse FFT analysis (Figure **S9**), the distribution of the different phases was explored and shows a clear Ni core surrounded primarily by NiO and smaller patches of $Ni(OH)_2$ (see Figure **5c**, additional images are shown in Figure **S11** and **S13**). Interestingly, no CrO_x overlayers were found surrounding any of the imaged Ni/NiO_x particles on both the as-prepared and used CrO_x-modified Ni/NiO_x-$Mg:SrTiO_3$. Nominally, there is no difference between the supported particles on either sample and particle growth that may result from the deposition of a CrO_x layer is absent.[13] Moreover, the Ni/NiO_x particles are barely distinguishable from that on Ni/NiO_x-$Mg:SrTiO_3$ (see **Figures S12 and S14** for HRTEM images) suggesting the Cr incorporation is very subtle and may indeed be present in mixed oxide species.

To further examine the CrO_x-modified Ni/NiO_x-$Mg:SrTiO_3$ photocatalysts STEM was used and EDX and EELS (see supporting information Figure **S15**) spectra were collected from the surface and the bulk of the material. In total, fifteen regions over the surface containing Ni/NiO_x particles, ten areas of the $Mg:SrTiO_3$ surface without supported particles, and seven entire aggregates (*i.e.*, bulk) were inspected by EDX. Due to the low Cr signal (and Mg) in each individual EDX spectra, the different groups of spectra were summed and are displayed in **Figure 4e**. In all summed EDX spectra, the Cr signal is weak while the Ni signal is expectedly strong at regions of the surface containing Ni/NiO_x particles. Considering that each spectrum contains a baseline Cr signal originating from constant objective lens pole piece excitation by X-rays emitted from the respective sample, Cr and Ni signals were normalized (for normalization procedure see supporting information). Figure **6** compares the integrated normalized Ni and Cr signals for EDX spectra collected from the bulk (Figure **6a**), Ni/NiO_x particles (Figure **6b**), and the $Mg:SrTiO_3$ surface (Figure **6c**). In addition, the Cr/Fe ratio (*i.e.*, a ratio of the normalized Cr and Fe signals) for all spectra is shown in Figure **S16.** In all spectra collected from regions containing Ni/NiO_x particles, the normalized Ni signal is about 3-40 times greater (left y-axis in Figure 6), than the average normalized Cr signal found in the bulk or at the bare $Mg:SrTiO_3$ surface (Figure **6**, see also supporting information for additional information). Note that for clarity the baseline Cr signal attributed to the pole piece fluorescence, the mean and average error ($7.22x10^{-2} \pm 2.37x10^{-2}$) of the integrated Cr signal associated with the bulk measurements is plotted (yellow areas) on all three graphs.

For about half of the regions possessing Ni/NiO_x particles (*i.e.*, spectra 2-3 and 11-15) also significant contributions of Cr were obtained. Interestingly, a very high Ni signal does not always correlate with a high Cr signal as revealed in spectra 8 and 11 (see Figure **6b** and also Figure **S17** comparing EDX data of spectra 8 and 15). Since roughly half (6 out of the 15 areas inspected with Ni/NiO_x particles) contain additional Cr content beyond the background level, this implies that the photodeposition of CrO_x onto Ni/NiO_x has not been consistent for all particles. Finally, the low integrated Cr signal (Figure **6c**) and Cr/Fe ratios (Figure **S16**) from regions of the $Mg:SrTiO_3$ surface are similar to that of the bulk, which further supports that CrO_x was deposited preferentially onto several, likely specific Ni/NiO_x particles, rather than uniformly throughout the surface. In contrast, the Mg peak is equal in all summed spectra indicating a

homogenous distribution of Mg throughout the bulk and surface of the support particles. The amount of Mg incorporated into the particles is consistent with a composition of $Mg_{0.03}Sr_{1.25}TiO_3$ according to EDX simulations done with NIST's DTSA-II software (Figure **S18**).

One can draw a few interesting and summarizing conclusions from the characterization and especially the EDX analysis. First, a dramatic effect in photocatalytic efficiency is observed, despite the small amount of Cr present and the absence of a continuous CrO_x layer or coating. Likely a mixed-Ni-Cr oxide is formed on the nano-scale. Secondly, the heterogeneity of the Cr distribution and loading on the Ni/NiO_x suggests that there are vast opportunities for further improvement of photocatalyst. Specifically, an increase in performance can be expected by achieving a more uniform distribution of CrO_x in contact with the NiO_x/Ni particles. Two hypotheses can be proposed to explain the presence of CrOx in the vicinity of some, and the absence in the vicinity of others. First, the revealed heterogeneity in CrO_x distribution may result from differences in the NiO_x shell thickness. Very thick shells (which are probably insulating) may prevent photogenerated electrons to transfer from the Mg:doped $SrTiO_3$ semiconductor to the deposited Ni/NiO_x particles, preventing reduction of Cr(VI)-ions in the photodeposition procedure. Conversely, any cracks within the NiO_x shell would expose the Ni metal and promote photodeposition. The consistent shell thickness and continuity of the NiO shells in several images, however, does not strongly support this hypothesis. Another explanation for inhomogeneity, might be difference in the interfacial/electrical contact between the Ni/NiO particles and the Mg:$SrTiO_3$ support. Poor contact could also impede photodeposition from occurring. A similar effect has been observed on Ni/NiO core/shell structures on TiO_2 wherein the photocatalyst deactivates due to a photochemical reaction causing Ni to dissolve into solution.[20] In this case, only a fraction of the particles exhibited the Ni leaching which was believed to result from the good electrical contact between the light-absorbing TiO_2 support and Ni particles. Several supported particles on the Mg:$SrTiO_3$ supports studied here were characterized by low contact angles (see **Figures S10-14**), indicative of a strong interfacial contact that likely facilitates charge transport. As such it even seems likely that a poor electrical interfacial contact between the Ni particles and the perovskite support will not only limit the photodeposition of CrO_x but will also limit the water splitting activity. In summary, improved catalyst preparation techniques aimed at establishing excellent contact between Ni/NiO_x and (doped) $SrTiO_3$ phases, may result in further enhancement of the photocatalytic activity.

Accessing Photocatalyst Stability

We will now address the beneficial effect of CrO_x on the stability of the catalyst. Sophisticated *in situ* ICP-MS analysis of dissolution of various elements is therefore required,[27,32] and was combined with *ex situ* analyses.[22,24] Three different photocatalysts were analyzed by in situ ICP-MS, namely Ni/NiO_x-$SrTiO_3$, Ni/NiO_x-Mg: $SrTiO_3$ and CrO_x-modified Ni/NiO_x-Mg:$SrTiO_3$, to understand the influence of Mg and CrO_x in more detail. These are shown in Figure 7.

It is immediately evident that Sr leaches rapidly from all samples (Figure **7a**). In fact rapid leaching occurs primarily upon contacting with water (Figure **S19** and Figure **S20**). Interestingly, Sr dissolution is most significant for Ni/NiO_x-Mg:$SrTiO_3$, suggesting that the presence of Mg promotes formation of an unstable surface structure. After photodeposition of CrO_x the quantity of Sr dissolution from Ni/NiO_x-Mg:$SrTiO_3$ is reduced significantly. The fraction of Sr accumulated in 5 minutes of illumination at 385 nm is comparatively small (Figure **7b**), and the relative amounts for the three investigated semiconductor composites are similar as compared to the total accumulated amount of dissolved Sr. Detected quantities of Cr, Ni, and Mg were comparatively low and no Ti was detected for all photocatalyst composites tested. Similarly to Sr dissolution, Mg leaching appeared to be reduced after photodeposition of CrO_x. It is important to emphasize that initiating and terminating illumination did not result in significant transients in Sr dissolution or other elements.

In Figure **7c** dissolution of Ni is summarized. Dissolution of Ni is rapid and predominant in the first 10 minutes of aqueous flow (dark). Interestingly, dissolution of Ni is significantly lower for Mg-containing photocatalysts as compared to Ni/NiO_x-modified $SrTiO_3$ (stoichiometric), suggesting that Mg stabilizes the interaction of Ni/NiO_x with the surface of the semiconductor, in agreement with the previously discussed electron microscopy data. The addition of CrO_x appears to further enhance Ni stability against leaching, although it is important to emphasize that leaching of the most instable Ni particles might have also occurred during the CrO_x-photodeposition procedure.

The results obtained by *in situ* ICP-MS regarding Ni dissolution are supported by *ex situ* ICP-OES analysis of the filtered solutions obtained at different times of activity testing (Figure 8). Though the overall amount of dissolved material is still low, again the largest quantities of dissolved Ni were determined for Ni/NiO_x-$SrTiO_3$. Interestingly, following Ni^{2+} quantities in solution during testing of Ni/NiO_x-Mg:$SrTiO_3$, suggested that some Ni^{2+} is redeposited/adsorbed in the absence of light.

During illumination the determined quantity of dissolved Ni is significantly lower compared to the initial phases of testing, i.e. reactor purging before illumination (Figure **8a**, blue bars). For all CrO_x-modified photocatalysts, leaching of Ni is clearly less pronounced and appeared to be constant already after 3 hours of exposure to the solution while purging (brown and yellow bars in Figure **8a**). Ni leaching is even further suppressed for Mg-containing Mg:$SrTiO_3$ materials (yellow bars). Focusing on the Mg content in the solution, the presence of Ni/NiO_x suppressed Mg dissolution (compare green and blue bars in Figure **8b**). Addition of CrO_x further suppresses Mg-leaching, which is otherwise most significant after illumination (after measurement).

Summarizing, *in situ* and *ex situ* ICP analysis show that: i) Sr leaching is significant for $SrTiO_3$ and even more so for Mg:$SrTiO_3$, ii) Mg is also found in solution, of which the quantity is smaller after photodeposition of CrO_x, iii) leaching of Ni is significantly reduced for Mg-containing $SrTiO_3$, and iv) photodeposition of CrO_x further reduces leaching of Ni/NiO_x.

Considering these results and the provided TEM analysis, we propose that mixed metal-oxides are formed, i.e. containing Ni and Cr, likely anchored with low contact angles on surfaces terminated by Mg-containing crystal orientations. The establishment of such conformations, is likely a function of leaching phenomena occurring during photodeposition. Certainly, the implications of dissolution on the performance and stability of photocatalysts used for overall water splitting (or CO_2 reduction) in aqueous media are of great importance to guide material development and industrial applicability of photocatalysts.

Conclusion

This work demonstrates, using state of the art high resolution microscopy and (*in situ*) elemental ICP analysis to follow metal dissolution, that stability of complex heterogenous photocatalysts can be improved by additives, only present in traces. We have demonstrated that active co-catalyst phases of Cr and Ni are likely formed, preferably at locations with low contact angles between Ni/NiO core shell particles and the Mg:$SrTiO_3$ surface, allowing effective charge transfer during the photodeposition procedure of CrO_x. Stability metrices such as metal dissolution are proposed here to be implemented in ongoing research to find efficient and durable photocatalysts to drive overall water splitting.

Declarations

ASSOCIATED CONTENT

Supporting Information. Additional photocatalytic activity and stability data (Fig. S1-S4), Raman, XRD and XPS analysis (Fig. S5-S8), supporting HRTEM images (Figure S9-S13), STEM-EELS (Figure S14), and STEM-EDX (Figure S15-S17) results.

AUTHOR INFORMATION

Corresponding Author

*Email: g.mul@utwente.nl; b.t.mei@utwente.nl

Present Addresses

†Inorganic Chemistry and Catalysis, Debye Institute for Nanomaterials Science, Utrecht University, 3854 CG, Utrecht, The Netherlands

Author Contributions

The manuscript was written through contributions of all authors. All authors have given approval to the final version of the manuscript. ‡These authors contributed equally.

Funding Sources

The China Scholarship Council is gratefully acknowledged for financially supporting Kai Han.

ACKNOWLEDGMENT

T.L.M. Velthuizen is acknowledged for assistance with XRF analysis and the Catalytic Process Materials group at the University of Twente for providing access to the XRF equipment. Haiber (DH) and P.A. Crozier (PAC) gratefully acknowledge the financial support from the U.S. Department of Energy (DE-SC0004954), the John M. Cowley Center for High Resolution Electron Microscopy, the Eyring Materials Center. DH and PAC also acknowledge assistance from Dr. Barnaby Levin for performing DTSA EDX simulation and assistance and discussion of STEM analysis.

Abbreviations

XRD, x-ray diffraction; XPS, x-ray photoelectron spectroscopy; TEM, transmission electron microscopy; EDX, energy-dispersive x-ray; ICP, inductively coupled plasma; MS, mass spectrometry; OES, optical emission spectrometry.

References

(1) Chiang, T. H.; Lyu, H.; Hisatomi, T.; Goto, Y.; Takata, T.; Katayama, M.; Minegishi, T.; Domen, K. Efficient Photocatalytic Water Splitting Using Al-Doped $SrTiO_3$ Coloaded with Molybdenum Oxide and Rhodium–Chromium Oxide. *ACS Catal.* **2018**, 2782–2788. https://doi.org/10.1021/acscatal.7b04264.

(2) Lyu, H.; Hisatomi, T.; Goto, Y.; Yoshida, M.; Higashi, T.; Katayama, M.; Takata, T.; Minegishi, T.; Nishiyama, H.; Yamada, T.; Sakata, Y.; Asakura, K.; Domen, K. An Al-Doped SrTiO 3 Photocatalyst Maintaining Sunlight-Driven Overall Water Splitting Activity for over 1000 h of Constant Illumination. *Chem. Sci.* **2019**, *10* (11), 3196–3201. https://doi.org/10.1039/c8sc05757e.

(3) Han, K.; Lin, Y.-C.; Yang, C.-M.; Jong, R.; Mul, G.; Mei, B. Promoting Photocatalytic Overall Water Splitting by Controlled Magnesium Incorporation in SrTiO 3 Photocatalysts. *ChemSusChem* **2017**, *10* (22), 4510–4516. https://doi.org/10.1002/cssc.201701794.

(4) Zhao, Z.; Goncalves, R. V.; Barman, S. K.; Willard, E. J.; Byle, E.; Perry, R.; Wu, Z.; Huda, M. N.; Moulé, A. J.; Osterloh, F. E. Electronic Structure Basis for Enhanced Overall Water Splitting Photocatalysis with Aluminum Doped SrTiO 3 in Natural Sunlight. *Energy Environ. Sci.* **2019**, *12* (4), 1385–1395. https://doi.org/10.1039/C9EE00310J.

(5) Ham, Y.; Hisatomi, T.; Goto, Y.; Moriya, Y.; Sakata, Y.; Yamakata, A.; Kubota, J.; Domen, K. Flux-Mediated Doping of SrTiO 3 Photocatalysts for Efficient Overall Water Splitting. *J. Mater. Chem. A* **2016**, *5* (0), 1–5. https://doi.org/10.1039/C5TA04843E.

(6) Takata, T.; Jiang, J.; Sakata, Y.; Nakabayashi, M.; Shibata, N.; Nandal, V.; Seki, K.; Hisatomi, T.; Domen, K. Photocatalytic Water Splitting with a Quantum Efficiency of Almost Unity. *Nature* **2020**, *581* (7809), 411–414. https://doi.org/10.1038/s41586-020-2278-9.

(7) Goto, Y.; Hisatomi, T.; Wang, Q.; Higashi, T.; Ishikiriyama, K.; Maeda, T.; Sakata, Y.; Okunaka, S.; Tokudome, H.; Katayama, M.; Akiyama, S.; Nishiyama, H.; Inoue, Y.; Takewaki, T.; Setoyama, T.; Minegishi, T.; Takata, T.; Yamada, T.; Domen, K. A Particulate Photocatalyst Water-Splitting Panel for Large-Scale Solar Hydrogen Generation. *Joule* **2018**, *2* (3), 509–520. https://doi.org/10.1016/j.joule.2017.12.009.

(8) Chen, S.; Takata, T.; Domen, K. Particulate Photocatalysts for Overall Water Splitting. *Nat. Rev. Mater.* **2017**, *2*, 17050. https://doi.org/10.1038/natrevmats.2017.50.

(9) Busser, G. W.; Mei, B.; Pougin, A.; Strunk, J.; Gutkowski, R.; Schuhmann, W.; Willinger, M.-G.; Schlögl, R.; Muhler, M. Photodeposition of Copper and Chromia on Gallium Oxide: The Role of Co-Catalysts in Photocatalytic Water Splitting. *ChemSusChem* **2014**, *7* (4), 1030–1034. https://doi.org/10.1002/cssc.201301065.

(10) Busser, G. W.; Mei, B.; Weide, P.; Vesborg, P. C. K.; Stührenberg, K.; Bauer, M.; Huang, X.; Willinger, M.-G.; Chorkendorff, I.; Schlögl, R.; Muhler, M. Cocatalyst Designing: A Regenerable Molybdenum-Containing Ternary Cocatalyst System for Efficient Photocatalytic Water Splitting. *ACS Catal.* **2015**, *5* (9), 5530–5539. https://doi.org/10.1021/acscatal.5b01428.

(11) Hisatomi, T.; Domen, K. Reaction Systems for Solar Hydrogen Production via Water Splitting with Particulate Semiconductor Photocatalysts. *Nat. Catal.* **2019**. https://doi.org/10.1038/s41929-019-0242-6.

(12) Maeda, K.; Teramura, K.; Lu, D.; Takata, T.; Saito, N.; Inoue, Y.; Domen, K. Photocatalyst Releasing Hydrogen from Water. *Nature* **2006**, *440* (7082), 295–295. https://doi.org/10.1038/440295a.

(13) Maeda, K.; Teramura, K.; Lu, D.; Saito, N.; Inoue, Y.; Domen, K. Roles of Rh/Cr2O3 (Core/Shell) Nanoparticles Photodeposited on Visible-Light-Responsive (Ga1-XZnx)(N1-XOx) Solid Solutions in Photocatalytic Overall Water Splitting. *J. Phys. Chem. C* **2007**, *111* (20), 7554–7560. https://doi.org/10.1021/jp071056j.

(14) Kanazawa, T.; Maeda, K. Light-Induced Synthesis of Heterojunctioned Nanoparticles on a Semiconductor as Durable Cocatalysts for Hydrogen Evolution. *ACS Appl. Mater. Interfaces* **2016**, *8* (11), 7165–7172. https://doi.org/10.1021/acsami.6b00907.

(15) Kurashige, W.; Mori, Y.; Ozaki, S.; Kawachi, M.; Hossain, S.; Kawawaki, T.; Shearer, C. J.; Iwase, A.; Metha, G. F.; Yamazoe, S.; Kudo, A.; Negishi, Y. Activation of Water-Splitting Photocatalysts by Loading

with Ultrafine Rh–Cr Mixed-Oxide Cocatalyst Nanoparticles. *Angew. Chemie Int. Ed.* **2020**, *59* (18), 7076–7082. https://doi.org/10.1002/anie.201916681.

(16) Domen, K.; Kudo, A.; Onishi, T.; Kosugi, N.; Kuroda, H. Photocatalytic Decomposition of Water into H2 and O2 over NiO-SrTiO3 Powder. 1. Structure. *J. Phys. Chem.* **1986**, *90* (26), 292–295. https://doi.org/10.1021/j100274a018.

(17) Townsend, T. K.; Browning, N. D.; Osterloh, F. E. Nanoscale Strontium Titanate Photocatalysts for Overall Water Splitting. *ACS Nano* **2012**, *6* (8), 7420–7426. https://doi.org/10.1021/nn302647u.

(18) Townsend, T. K.; Browning, N. D.; Osterloh, F. E. Overall Photocatalytic Water Splitting with NiOx–SrTiO3 – a Revised Mechanism. *Energy Environ. Sci.* **2012**, *5* (11), 9543. https://doi.org/10.1039/c2ee22665k.

(19) Han, K.; Kreuger, T.; Mei, B.; Mul, G. Transient Behavior of Ni@NiO x Functionalized SrTiO 3 in Overall Water Splitting. *ACS Catal.* **2017**, *7* (3), 1610–1614. https://doi.org/10.1021/acscatal.6b03662.

(20) Zhang, L.; Liu, Q.; Aoki, T.; Crozier, P. A. Structural Evolution during Photocorrosion of Ni/NiO Core/Shell Cocatalyst on TiO 2. *J. Phys. Chem. C* **2015**, *119* (13), 7207–7214. https://doi.org/10.1021/jp512907g.

(21) Zoontjes, M. G. C.; Han, K.; Huijben, M.; van der Wiel, W. G.; Mul, G. The Effect of Rh Δ+ Dopant in SrTiO 3 on the Active Oxidation State of Co-Catalytic Pt Nanoparticles in Overall Water Splitting. *Catal. Sci. Technol.* **2016**, *6* (21), 7793–7799. https://doi.org/10.1039/C6CY01424K.

(22) Knöppel, J.; Zhang, S.; Speck, F. D.; Mayrhofer, K. J. J.; Scheu, C.; Cherevko, S. Time-Resolved Analysis of Dissolution Phenomena in Photoelectrochemistry – A Case Study of WO_3 Photocorrosion. *Electrochem. commun.* **2018**, *96*, 53–56. https://doi.org/10.1016/j.elecom.2018.09.008.

(23) Klemm, S. O.; Topalov, A. A.; Laska, C. A.; Mayrhofer, K. J. J. Coupling of a High Throughput Microelectrochemical Cell with Online Multielemental Trace Analysis by ICP-MS. *Electrochem. commun.* **2011**, *13* (12), 1533–1535. https://doi.org/10.1016/j.elecom.2011.10.017.

(24) Zhang, S.; Rohloff, M.; Kasian, O.; Mingers, A. M.; Mayrhofer, K. J. J.; Fischer, A.; Scheu, C.; Cherevko, S. Dissolution of BiVO 4 Photoanodes Revealed by Time-Resolved Measurements under Photoelectrochemical Conditions. *J. Phys. Chem. C* **2019**, *123* (38), 23410–23418. https://doi.org/10.1021/acs.jpcc.9b07220.

(25) Maeda, K.; Teramura, K.; Lu, D.; Saito, N.; Inoue, Y.; Domen, K. Noble-Metal/Cr2O3 Core/Shell Nanoparticles as a Cocatalyst for Photocatalytic Overall Water Splitting. *Angew. Chemie - Int. Ed.* **2006**, *45* (46), 7806–7809. https://doi.org/10.1002/anie.200602473.

(26) Fabian, D. M.; Hu, S.; Singh, N.; Houle, F. a; Hisatomi, T.; Domen, K.; Osterloh, F. E.; Ardo, S. Particle Suspension Reactors and Materials for Solar-Driven Water Splitting. *Energy Environ. Sci.* **2015**, *8* (10), 2825–2850. https://doi.org/10.1039/C5EE01434D.

(27) Mei, B.; Han, K.; Mul, G. Driving Surface Redox Reactions in Heterogeneous Photocatalysis: The Active State of Illuminated Semiconductor-Supported Nanoparticles during Overall Water-Splitting. *ACS Catal.* **2018**, *8* (10), 9154–9164. https://doi.org/10.1021/acscatal.8b02215.

(28) Takanabe, K. Addressing Fundamental Experimental Aspects of Photocatalysis Studies. *J. Catal.* **2019**, *370*, 480–484. https://doi.org/10.1016/j.jcat.2018.10.006.

(29) Dionigi, F.; Vesborg, P. C. K.; Pedersen, T.; Hansen, O.; Dahl, S.; Xiong, A.; Maeda, K.; Domen, K.; Chorkendorff, I. Suppression of the Water Splitting Back Reaction on GaN:ZnO Photocatalysts Loaded with Core/Shell Cocatalysts, Investigated Using a μ-Reactor. *J. Catal.* **2012**, *292*, 26–31. https://doi.org/10.1016/j.jcat.2012.03.021.

(30) Takanabe, K. Photocatalytic Water Splitting: Quantitative Approaches toward Photocatalyst by Design. *ACS Catal.* **2017**, *7* (11), 8006–8022. https://doi.org/10.1021/acscatal.7b02662.

(31) Qureshi, M.; Takanabe, K. Insights on Measuring and Reporting Heterogeneous Photocatalysis: Efficiency Definitions and Setup Examples. *Chem. Mater.* **2017**, *29* (1), 158–167. https://doi.org/10.1021/acs.chemmater.6b02907.

(32) Spanu, D.; Minguzzi, A.; Recchia, S.; Shahvardanfard, F.; Tomanec, O.; Zboril, R.; Schmuki, P.; Ghigna, P.; Altomare, M. An Operando X-Ray Absorption Spectroscopy Study of a NiCu–TiO 2 Photocatalyst for H 2 Evolution. *ACS Catal.* **2020**, *10* (15), 8293–8302. https://doi.org/10.1021/acscatal.0c01373.

Figures

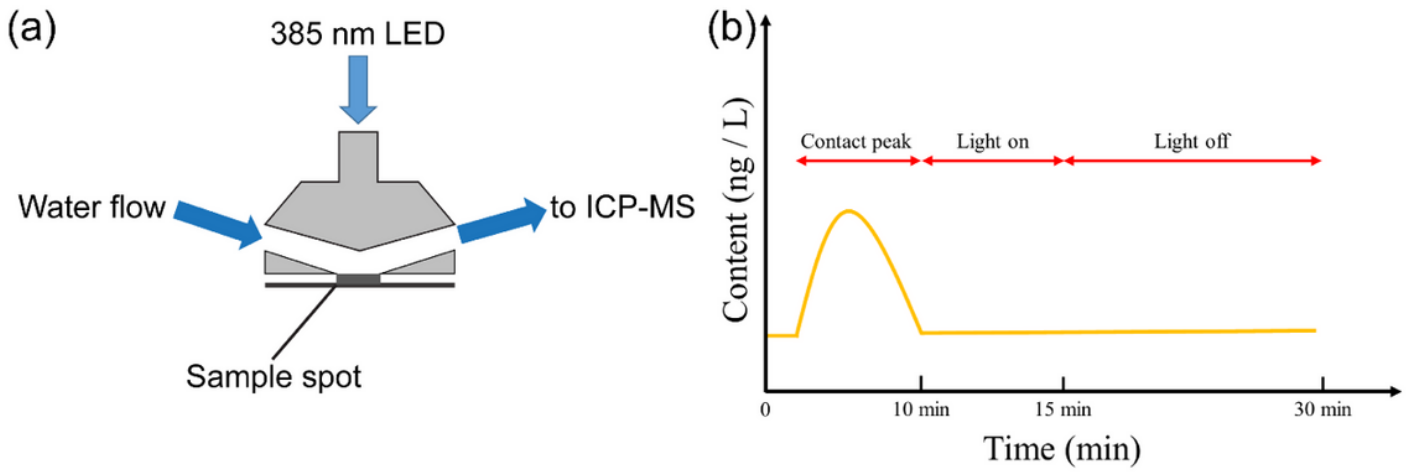

Figure 1

Schematic illustration of the applied ICP-MS measurement geometry (a) and the sequence of measurement (b). In the right figure the peak width of about 10 minutes realistically represents the actual concentration profile.

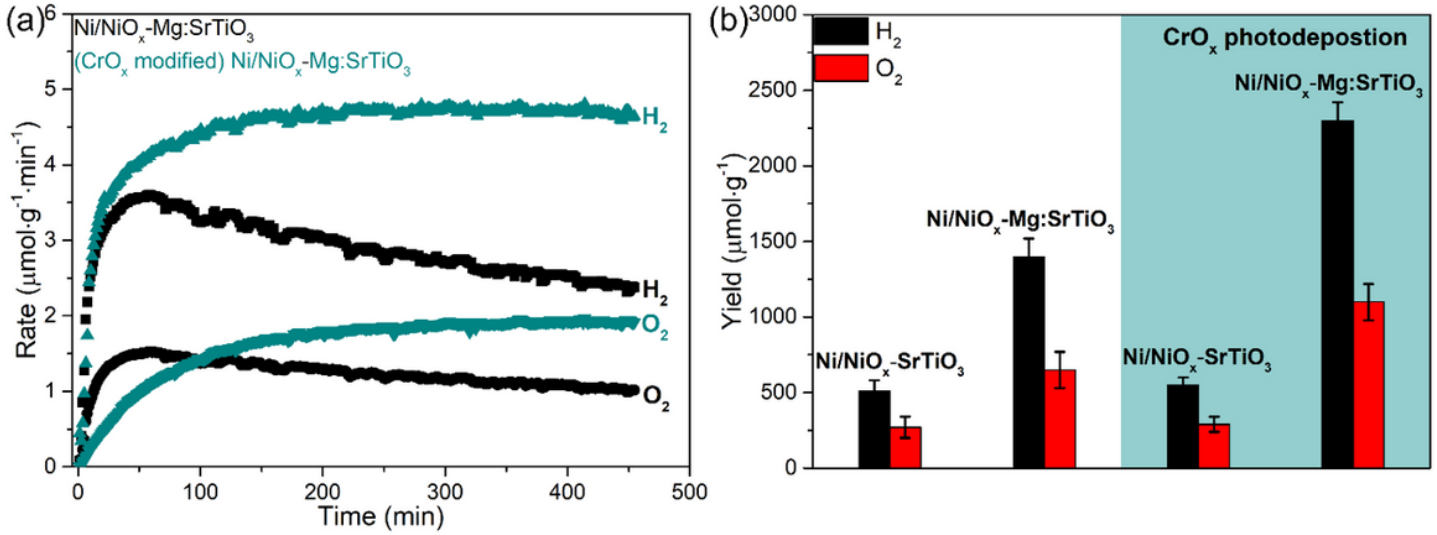

Figure 2

a) Time resolved photocatalytic water splitting performance of (CrOx-modified) Ni/NiOx-Mg:SrTiO3 composites using 365 nm LED light illumination. Reaction conditions: 25 mg catalyst in 25 mL DI water. b) Hydrogen and oxygen yields of Ni/NiOx-SrTiO3 and Ni/NiOx-Mg:SrTiO3 in the absence and presence of CrOx; constant illumination was applied for a period of 8 h. Reaction conditions: 25 mg catalyst in 25 mL DI water using 365 nm LED light.

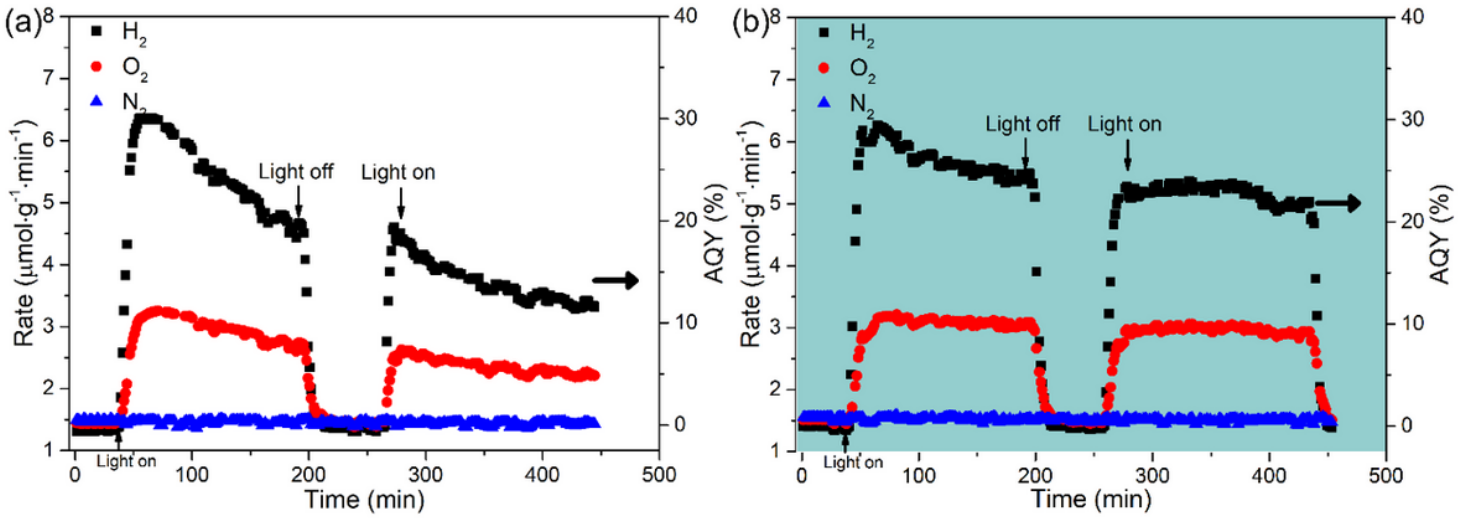

Figure 3

Photocatalytic activity of a Ni/NiOx-Mg:SrTiO3 (a) and CrOx modified Ni/NiOx-Mg:SrTiO3 (b) composite when a mixture of H2, O2 and N2 (all at 80 ppm) is used as purge gas. Reaction condition: 25 mg catalyst in 25 mL DI water with 365 nm LED as the light source.

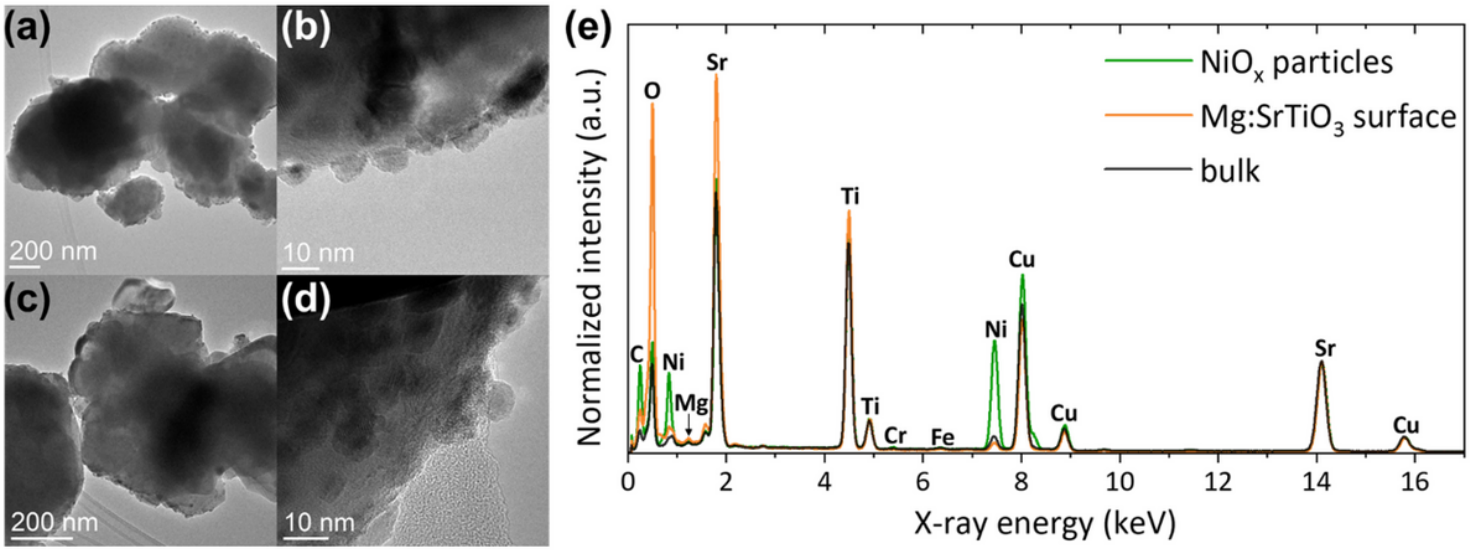

Figure 4

Survey TEM images of fresh Ni/NiOx-Mg:SrTiO3 composite (a, b) and fresh CrOx-modified Ni/NiOx-Mg:SrTiO3 composite (c, d). (e) Summed EDX spectra of the fresh CrOx-modified Ni/NiOx-Mg:SrTiO3 composite: Black line for bulk and green and orange lines for surface regions containing NiOx particles and no particles, respectively. (The Cu signal arises from the Cu TEM support grid and is not part of the sample).

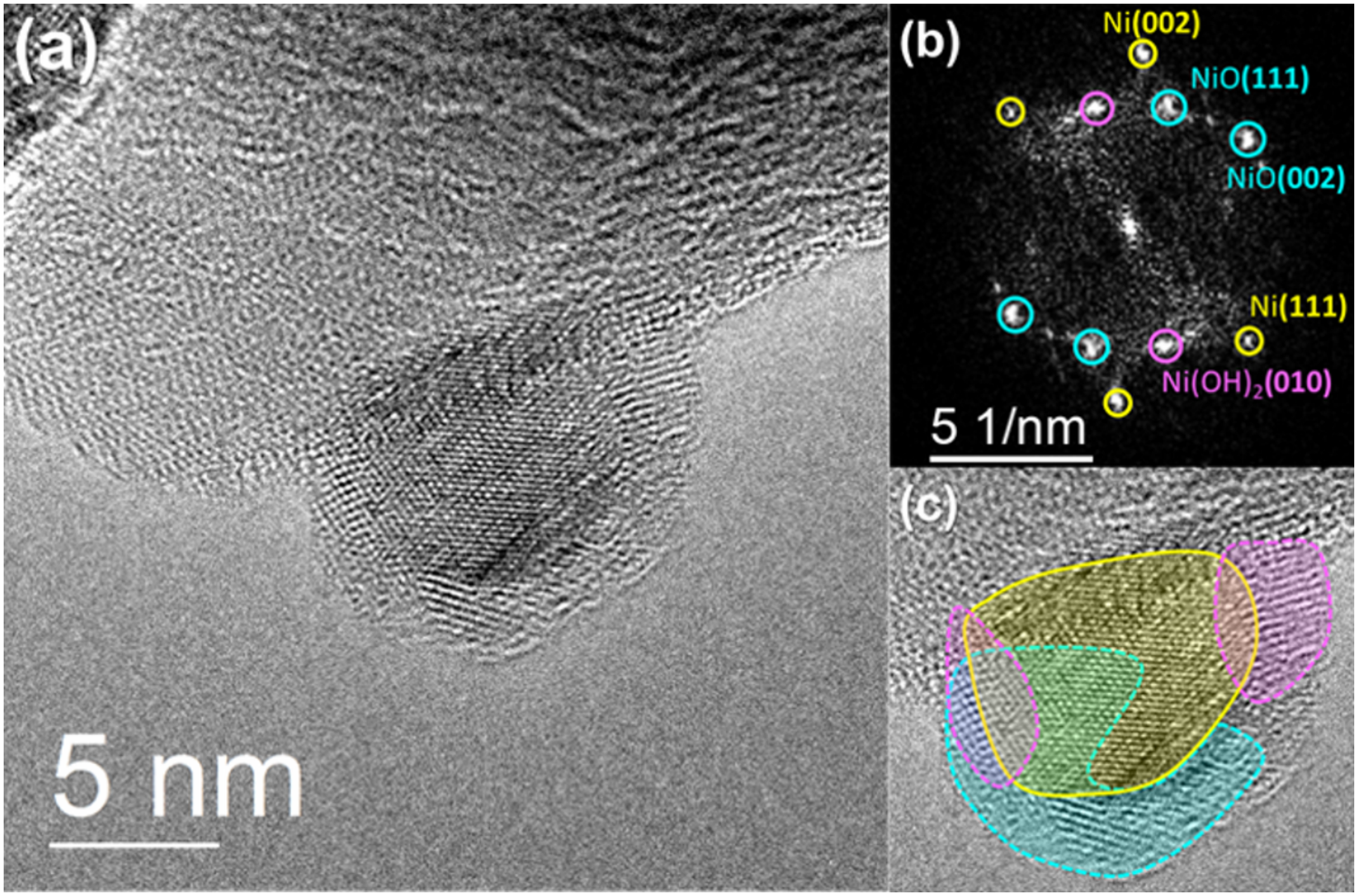

Figure 5

(a) HRTEM image of a typical Ni/NiOx core-shell particle of CrOx-modified Ni/NiOx-Mg:SrTiO3 with low contact angle. Similar images were obtained for Ni/NiOx-Mg:SrTiO3 in the absence of CrOx. (b) FFT from the region containing the supported core-shell particle with Ni, NiO, and Ni(OH)2 lattice spacings identified. (c) Regions of the core-shell particle containing Ni (yellow), NiO (blue), and Ni(OH)2 (pink) as identified using inverse FFTs of the individual diffraction spot pairs.

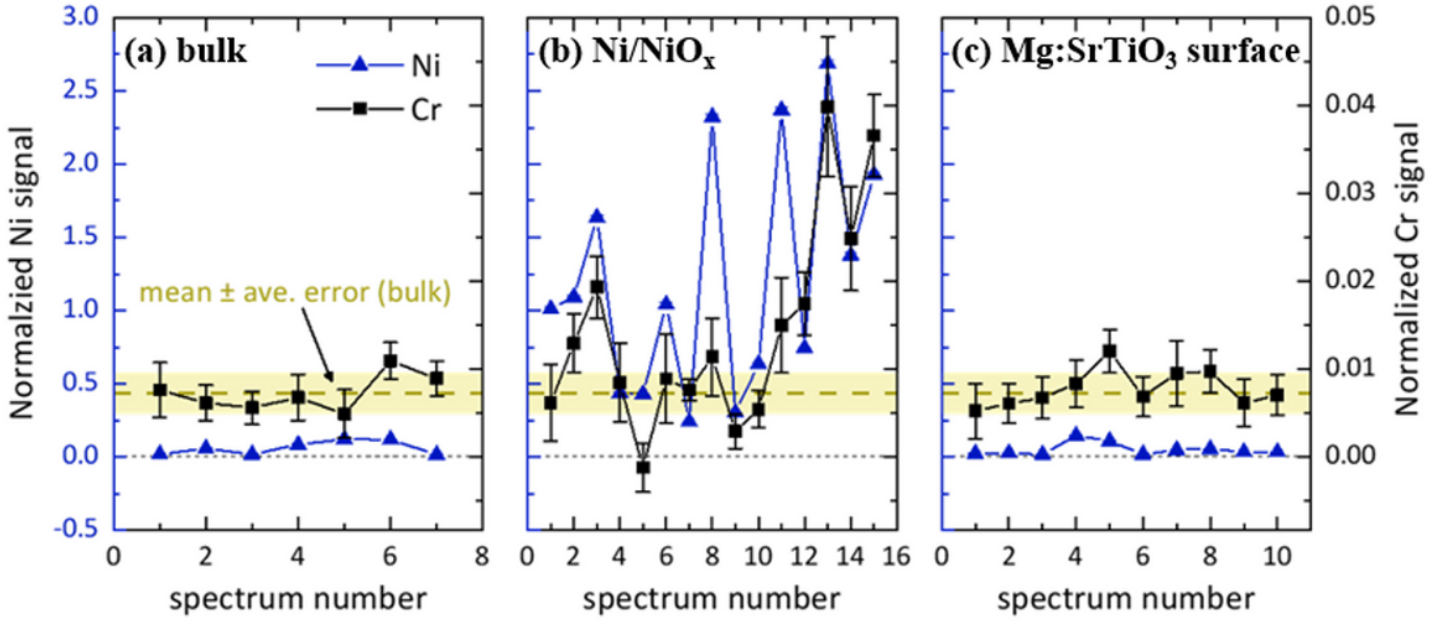

Figure 6

EDX signal analysis: Integrated and normalized Ni (left vertical axis, blue) and Cr (right vertical axis, black) signals determined in each individual spectrum from the bulk (a), supported NiOx particles (b), and the bare Mg:SrTiO3 surface (c). The mean and average error (7.22x10-2 ± 2.37x10-2) associated with the integrated Cr signal for the bulk, representing the pole piece fluorescence, is marked on each panel in gold/yellow.

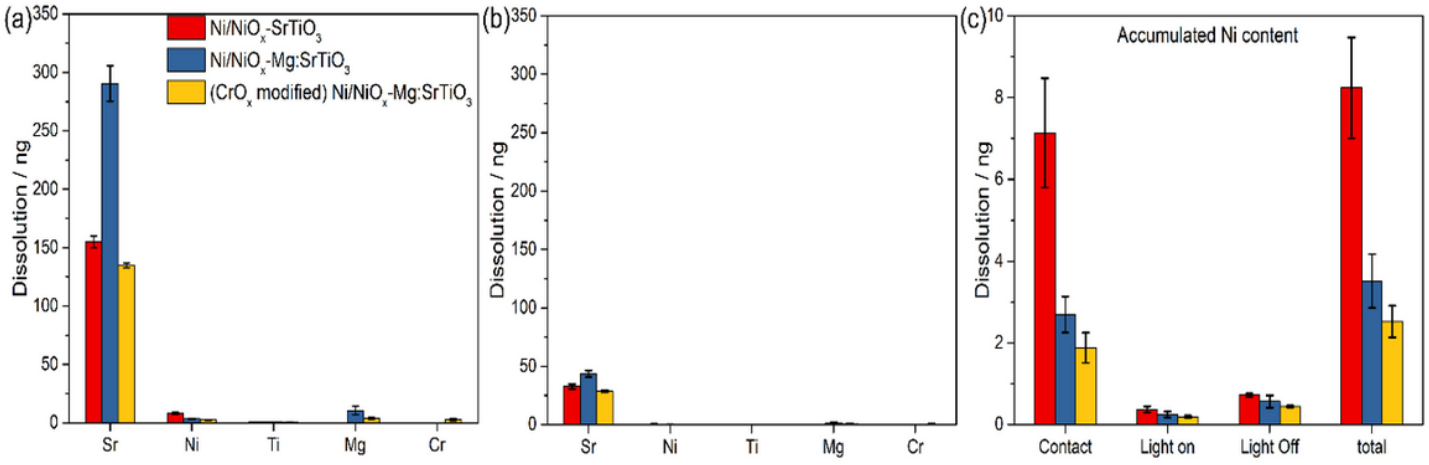

Figure 7

a) In situ ICP-MS results of accumulated liquid content after 30 minutes of exposure to the photocatalyst, consisting of an initial 10 minutes of aqueous flow in darkness, illumination for 5 minutes, and additional aqueous flow for 15 minutes in darkness. In Figure b) the accumulated amounts during 5 minutes of constant illumination, only are displayed. c) Accumulated Ni-content (note the different scale as compared to Figure a)) after 10 minutes of liquid flow ('contact'), 5 minutes of illumination ('light on'), 15 minutes of continuous flow ('light off') and the accumulated total after 30 minutes. Measurement conditions: 15 µg per catalyst and 186 µL/min of water flow.

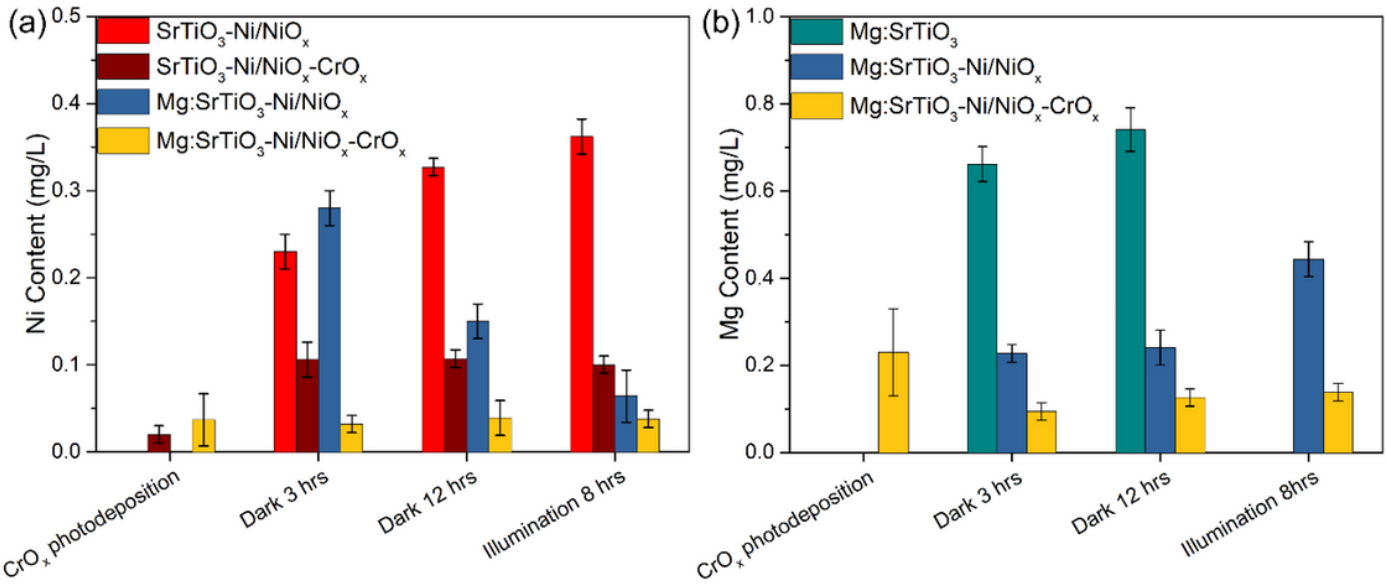

Figure 8

Ex situ ICP OES analysis performed at different stages of a typical photocatalytic water splitting experiment: (a) Ni and (b) Mg content. Reaction condition: 25 mg catalyst in 25 mL DI water. For each individual measurement solution was extracted from the reactor and filtered to remove photocatalyst particles.

Supplementary Files

This is a list of supplementary files associated with this preprint. Click to download.

- NatureCatalysisMgSTONiCrsupportinginformation.docx